International Journal of GEOMATE, July, 2020, Vol.19, Issue 71, pp. 160 - 165
ISSN: 2186-2982 (P), 2186-2990 (O), Japan, DOI: https://doi.org/10.21660/2020.71.9197
Geotechnique, Construction Materials and Environment

COMPARISON OF MACROPORE STRUCTURES AND NETWORKS OF AUTOCLAVED AERATED CONCRETE BLOCKS USING MICRO-FOCUS X-RAY COMPUTED TOMOGRAPHY

* Akihiro MATSUNO[1], Shin ISHIZUKA[1], Trong Lam NGUYEN[2], Nguyen Tien DUNG[2], Van Tuan NGUYEN[2], Hoang Giang NGUYEN[2], and Ken KAWAMOTO[1,2]

[1]Graduate School of Science and Engineering, Saitama University, Japan [2]National University of Civil Engineering, Vietnam

*Corresponding Author, Received: 19 May 2019, Revised: 29 Nov. 2019, Accepted: 16 March 2020

ABSTRACT: Autoclaved aerated concrete (AAC) is a lightweight cementitious material that has a unique structure characterized by a robust skeleton and pores (porous medium). The internal pore network structure of AAC highly controls mechanical and mass transport properties. This study aimed to identify the pore network structure of AAC (typical meso- and macropores with diameter >10 μm) and to correlate the pore characteristics with mass transport parameters of AAC such as gas diffusivity (D_p/D_0), air permeability (k_a), and saturated hydraulic conductivity (K_s) using three different AAC blocks. First, the three-dimensional macropore structure and network of 10 cm cubes of AAC blocks were visualized by microfocus X-ray computed tomography (MFXCT), and then pore structural parameters such as effective pore radius, coordination number, and tortuosity in the z direction were analyzed using a three-dimensional medial axis technique. Next, mass transport parameters were measured using 100 cm^3 core samples taken from AAC blocks. Based on measured pore structural parameters with a scanning resolution of 12 μm, clear differences in macropore networks were observed among tested samples: the AAC blocks from Vietnam had less tortuous macropores with smaller and narrower range of radii compared to Japanese AAC sample. In collaboration with predictive models for mass transport parameters, D_p/D_0, k_a, and K_s were estimated by using the pore structural parameters from MFXCT and compared to measured values. The estimated D_p/D_0 and k_a values fit the measured values for all tested samples well, but the estimated k_a and K_s from MFXCT under- or overestimated the measured values.

Keywords: Autoclaved aerated concrete (AAC), Pore network structure, Micro-focus X-ray CT system (MFXCT), Mass transport parameter

1. INTRODUCTION

Autoclaved aerated concrete (AAC) is a lightweight cementitious material that has a unique structure characterized by a robust skeleton and pores (porous media). Currently, AAC is widely used in many building applications all over the world due to its advantages such as low density, thermal conductivity and high heat resistance [1]. A typical process for the production of AAC includes hydrothermal treatment of a mixture of quartz sand, lime, cement, gypsum, and other additives at high temperature (typically 180–200°C) under saturated steam pressure, which results in the formation of crystalline calcium silicate hydrate, namely, tobermorite ($Ca_5Si_6(O, OH, F)_{18}5H_2O$) [2]. Due to the manufacturing process, multiple pores are generated.

Generally, the pore diameter (d) of AAC is classified into micropores of d <10 μm and meso- and macropores of $d \geq 10$ μm (hereafter simply termed macropores). The micropores contribute mainly to the layered structure of tobermorite [3]. Nguyen et al. (2018) measured pore size distributions of several AAC samples manufactured in Japan and Vietnam using mercury intrusion porosimetry (MIP) [4]. They observed a clear difference in the pore distributions in the range of micropores (typical d<10 μm) between AAC samples, but no significant difference in the range of macropores ($d \geq 10$ μm).

MIP is a useful tool to quantify the pore size, distribution, and volume; however, the measured data cannot give quantitative information on pore structure and network including pore tortuosity, coordination number, and isolated pores. Because the mass transport processes in AAC such as water imbibition, gas and vapor exchange, and heat conduction are highly controlled by pore structure and network, it is important to characterize the pore network structures and to understand the relationship to mass transport parameters such as gas diffusivity, air and water permeabilities, and thermal conductivity.

Nowadays, X-ray computed tomography (CT) has emerged as a powerful non-destructive tool for examining three-dimensional characteristics of pore geometry. In particular, micro-focus X-ray CT (MFXCT) is able to visualize and analyze the macropore network characteristics (typical pore with diameter >10 μm) [5,6,7]. In this study, therefore, the objectives were (i) to visualize the macropore network structures of AAC samples using MFXCT and analyze the pore structural parameters, and (ii) to examine the relationships between estimated mass transport parameters based on the X-ray CT analysis and measured values.

2. MATERIALS AND METHODS

2.1 AAC samples

Three different AAC blocks manufactured in Japan and Vietnam used in this study. One was from Japan (hereafter labeled JP) and two from Vietnam (hereafter labeled VN1 and VN2). The detailed material properties were given in [4].

First, the AAC blocks were cut to approximately 10-cm cubes, and the exact volume and weights at both air-dried and oven-dried conditions were measured. By using the measured dry bulk density (ρ_d) and specific gravity (G_s) of samples, we calculated the total porosity (ϕ) of the tested samples. Then, the samples were fully saturated. After measuring the sample weight at saturation, the samples were put in a pressure chamber and drained at 300 cm H_2O of suction (h). Based on the relationship of equivalent pore diameter, d_{eq} (μm), and h (cm H_2O), $d_{eq} = 3000/h$ [8], the water retained in the macropores ($d \geq 10$ μm) was drained at equilibrium. By measuring the weight of samples at $h = 300$ cm H_2O, the air-fill at $h = 300$ cm H_2O, ε_{300}, was calculated. Because water retained porosity in micropores at $h = 300$ cm H_2O, the measured ε_{300} represents the macro porosity of tested samples.

In order to measure mass transport parameters, 100 cm^3 core samples were taken from AAC blocks. The core samples were put into an acrylic cylinder 15 cm in diameter and 10 cm in height. The gap between the sample and acrylic cylinder was filled completely with paraffin. The gas diffusivity (D_p/D_0) and air permeability (k_a) were measured using air-dried core samples, and saturated hydraulic conductivity (K_s) was measured using a water-saturated core sample. The measurement methods of mass transport parameters are given in [5,6,9].

2.2 MFXCT scanning and analysis

Pore network structures were visualized using a MFXCT system (inspeXio SMX-90CT, Shimadzu Co. Ltd. Japan) with 90 kV and 110 μA of energy. The scanning and analysis conditions are: view number = 1800, average number for scanning = 4, image size of slice = 1024 × 1024 pixels, and scaling factor = 150. In this study, three different scanning resolutions (SR), 12, 30, and 50 μm/voxel, were applied and corresponding field of views (FOV) became FOV (XY) = 12.3, 30.7, and 51.2 mm and FOV (Z) = 6.5, 16.2, and 27.0 mm. The total number of slices used to construct a three-dimensional image was 541.

Scanned CT images of tested samples were reconstructed and then binarized (black and white image) with a threshhold value of measured ε_{300} to analyze macropore networks in tested samples (see Fig. 1). After image binarization, the medial axis skeleton for the pore space was constructed based on the three-dimensional medial axis (3DMA) technique using ExFact VR 2.1 (Nihon Visual Science Inc., Japan). Then, the 3DMA skeleton images were used to determine the pore structure parameters of the macropore network, including distributions of effective pore radius (r_{eff}), coordination number (N), and tortuosity (T_{zz}), setting the region of interest (ROI; analysis volume) to 300×300×300 voxels.

3. RESULTS AND DISCUSSION

3.1 Basic physical properties of AAC samples

Basic physical properties of tested AAC samples are summarized in Table 1. The measured ϕ values were similar and ranged between 0.77 and 0.80. On the other hand, the ε_{300} values (macroporosities) varied depending on the tested samples, and VN1 gave the highest macroporosity among tested samples.

Table 1 Basic physical properties of tested AAC samples.

Sample	ρ_d (g/cm^3)	G_s	ϕ	ε_{300}
JP	0.50	2.15	0.77	0.34
VN1	0.53	2.71	0.80	0.46
VN2	0.62	2.51	0.77	0.37

3.2 Pore network structure of AAC samples

Binarized images of tested AAC samples scanned with three SR values are shown in Fig. 1. In the images, black zones indicate macropores ($d \geq 10$ μm) and white zones indicate solid parts including micropores with $d < 10$ μm. Figure 2 exemplifies three-dimensional reconstructed images, medial axis skeleton for macropores, and shortest paths in the ZZ direction for tested AAC samples. Here, the shortest paths ZZ represent the

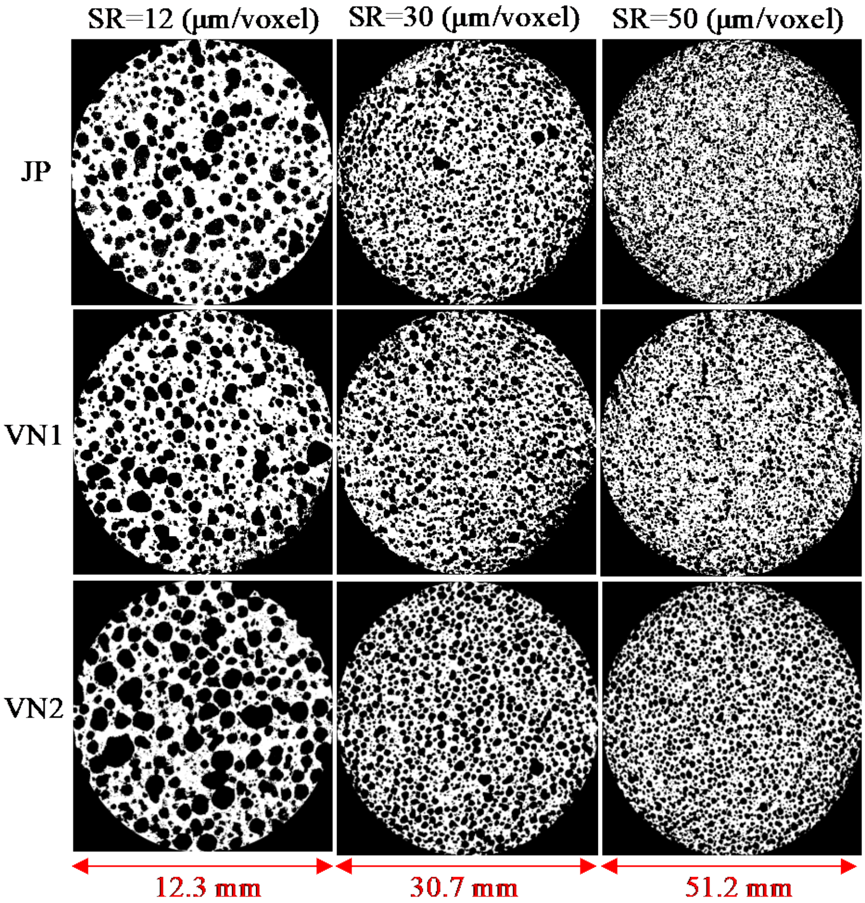

Fig. 1 Binalized images for tested AAC samples with three scanning resolutions (SR).

	3D Model	MA (Medial Axis)	Shortest Paths	Isolated pore (%)
JP	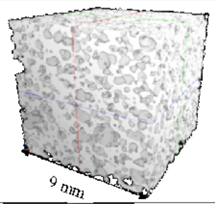	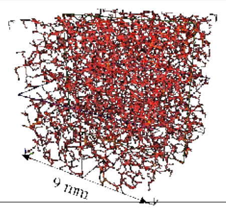	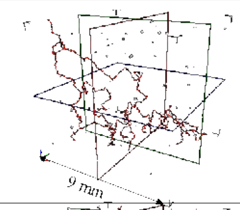	39
VN1	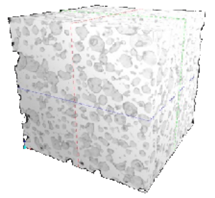	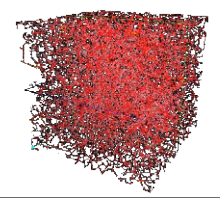	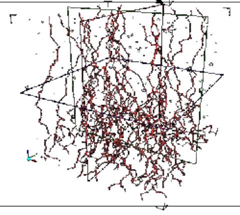	1.2
VN2	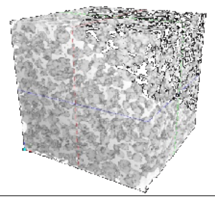	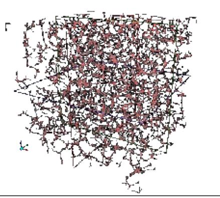	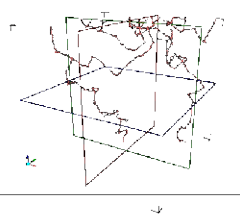	13

Fig. 2 Three-dimensional reconstructred images, medial axis skelton for macropores, shortest paths in ZZ direction, and isolated pores (%) for tested AAC samples (SR = 30 μm/voxel, ROI = 300×300×300).

extracted connected pores passing from one side to the other side in the ZZ direction (except for isolated pores). A big difference among tested AAC samples was observed in the shortest paths. For JP AAC, the connected macropores that give the shortest paths were lower than those for VN AAC samples, resulting in a higher number of isolated pores (39.0%) compared to those for VN AAC (1.2% and 13.0%).

Figure 3 explemplifies the measured probability density data of pore structural parameters (r_{eff} of JP AAC scanned with SR = 30 μm/voxel). First, three ROIs with 300 × 300 × 300 voxels inside the reconstructed binarized image were choosen arbitrarily, and three probability densities were measured. Then, either a normal or log-normal distribution curve was fitted to the measured probability density data after examining statistical tests inlcuding the Shapiro-Wilk test, ANOVA test, and Kruskal-Wallis test ([6,7,10]). Based on the statistical tests, it was found that r_{eff} was fitted to a normal distribution curve while N and T_{zz} were fitted to normal distribution curves.

Measured normal and log-normal distributions for pore structural parameters (r_{eff} , N, and T_{zz}) with three SR values are shown in Fig. 4. Mean (μ) and standard deviation (σ) of measured pore structural parameters for tested samples are summarized in Table 2.

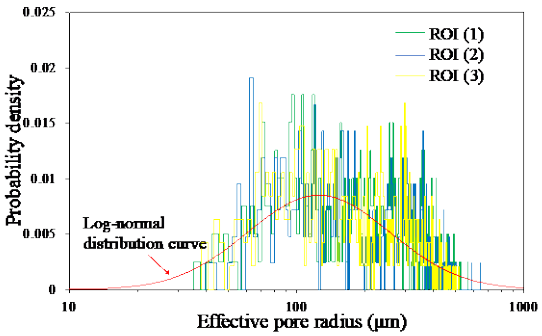

Fig. 3 Measured probability densities of effective pore radius (r_{eff}) from three ROIs for JP AAC.

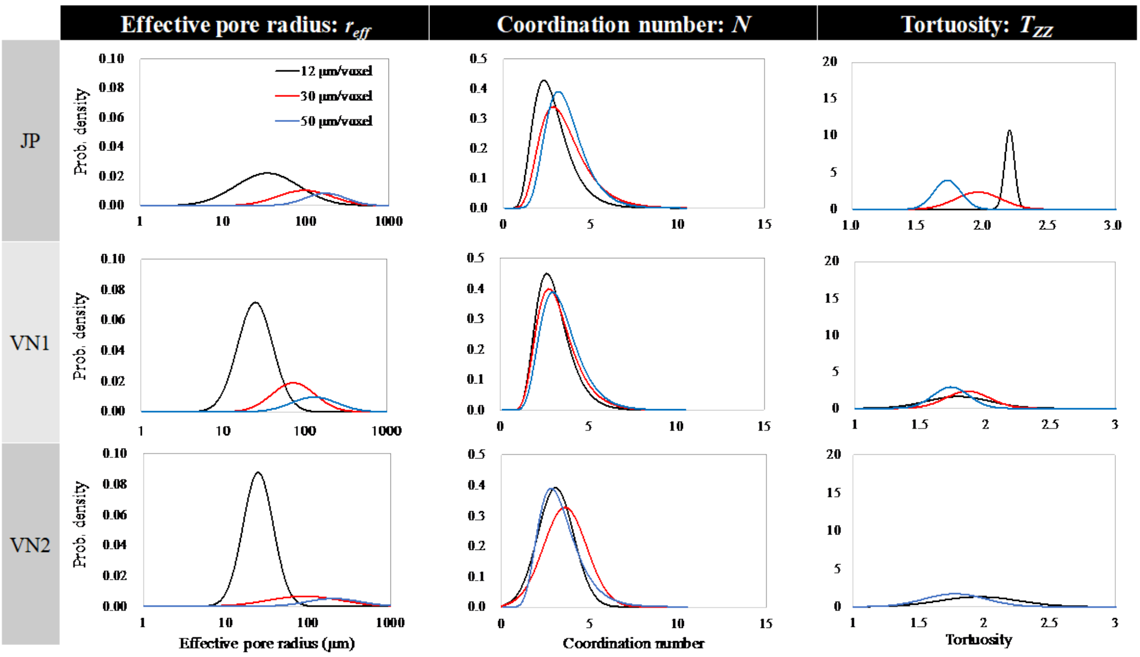

Fig. 4 Measured log-normal distribution curves of r_{eff} and normal ditribution curves of N and T_{zz} for tested AAC samples. Note that the normal distibution curve did not fit the measured probability density of T_{zz} for VN2 (SR = 30 μm/voxel).

Table 2 Summary of pore structural parameters (r_{eff} , N, and T_{zz}) with three SR values. Mean (μ) and standard deviation (σ) are given.

	SR=12 μm/voxel						SR=30 μm/voxel						SR=50 μm/voxel					
	r_{eff}		N		T_{ZZ}		r_{eff}		N		T_{ZZ}		r_{eff}		N		T_{ZZ}	
	μ	σ	μ	σ	μ	σ	μ	σ	μ	σ	μ	σ	μ	σ	μ	σ	μ	σ
JP	46.2	52.6	2.55	0.86	2.20	0.04	142.9	115.4	3.01	1.23	1.96	0.17	222.6	123.6	3.35	1.04	1.72	0.10
VN1	28.0	15.3	2.79	0.88	1.79	0.24	123.3	54.7	3.60	1.22	1.87	0.17	150.9	121.1	3.09	1.05	1.74	0.14
VN2	27.5	12.3	1.97	1.02	1.96	0.31	192.6	203.9	1.38	0.28	1.96	0.02	297.7	210.1	1.52	1.19	1.78	0.24

As shown in Fig. 4, the measured r_{eff} values were highly affected by SR values. Normally, the mean r_{eff} increased with increasing in SR values, indicating that scanning with large SRs of 30 and 50 μm/voxel overestimated the size of macropores because of the deviation between the target pores (typical $d \geq 10$ μm) and the scanning resolution. Comparing the measured r_{eff} of JP and VN AAC samples with SR = 12 μm/voxel, JP AAC gave a larger pore (mean: 46.2 μm) than those of VN AAC (mean: 27.5–28.0 μm). In addition, the distributions of r_{eff} of VN AAC samples became narrower than JP AAC. It is supposed that the differences between AAC manufacturing processes of Japan and Vietnam cause the difference in macropore network structures of AAC blocks.

On the other hand, there was a small difference in measured N between JP and VN AAC samples, and the measured N values did not depend on SR values. The measured N for VN2 (mean: 1.38–1.97) became slightly lower than those from JP and VN1 samples (mean: 2.55–3.60). Because the N value means the number of surrounding connected pores, VN2 has fewer connected macropores (i.e., more isolated macropores) than other AAC samples. The measured T_{zz} values for VN1 and VN 2 (mean: 1.74–1.96) were lower than those for JP (mean: 1.72–2.20), suggesting that the macropores of VN AAC samples were less tortuous (i.e., straighter) than those of JP AAC.

3.3 Correlation between measured and estimated mass transport parameters from MFXCT analysis

In collaboration with predictive modes for mass transport parameters, [6] estimated D_p/D_0, k_a, and K_s using measured pore structural parameters from MFXCT. For estimating D_p/D_0 and k_a, the Buckingham model [11,12] was applied combined with measured mean T_{zz} values (SR = 12 μm/voxel) from MFXCT analysis. For estimating K_s, the Kozeny-Carman model [13,14] was applied combining MFXCT-driven surface area and total porosity (ϕ).

A comparison of measured and estimated mass transport parameters from MFXCT analysis is shown in Fig. 5. For D_p/D_0, the estimated values from MFXCT analysis for all tested samples fitted well the measured values, suggesting that the mean T_{zz} values from MFXCT are very useful to predict gas diffusivities of AAC samples (Fig. 5a). For k_a, the estimated values of VN AAC samples captured the measured values well. However, the estimated k_a of JP AAC was around two times higher than the measured value (Fig. 5b). This might be attributed to the higher tortuosity of JP AAC (SR = 12 μm/voxel in Fig. 4). For K_s, the estimated values of JP AAC fitted well to the measured value, but the estimated values of VN AAC samples overestimated the measured K_s values ranging from 1:2.5 to 1:3.0 (Fig. 5c).

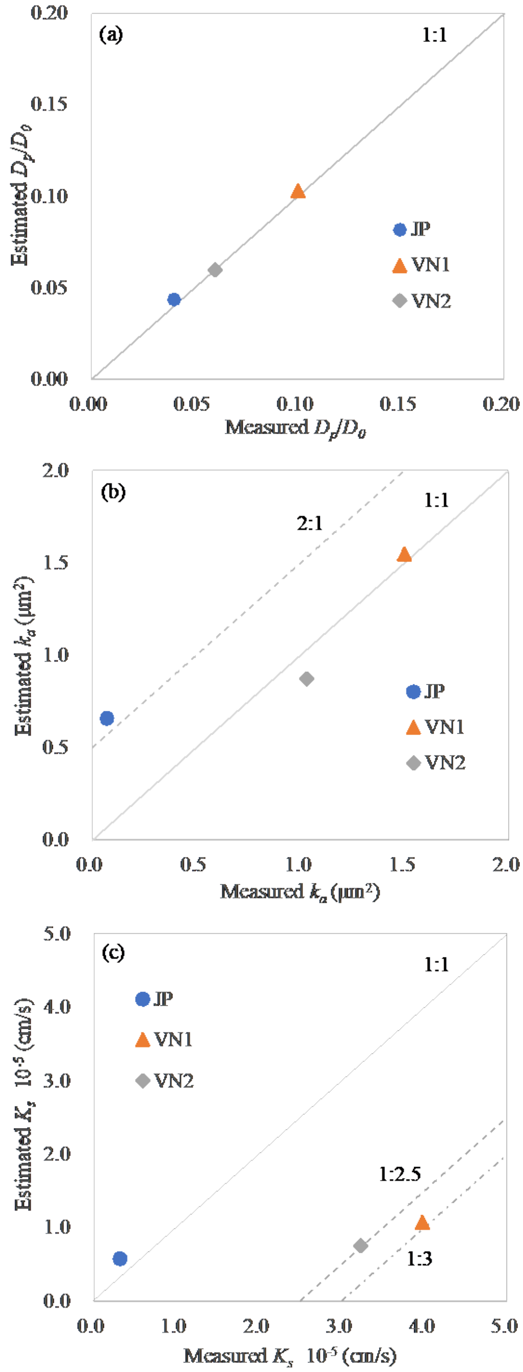

Fig. 5 Comparisons of measured and estimated mass transport parameters from MFXCT analysis. (a) gas diffusivity (D_p/D_0), (b) air permeability (k_a), and (c) saturated hydraulic conductivity (K_s).

Overall, the test results showed that the estimation of mass transport parameters for AAC samples from MFXCT analysis is likely to be within the range of acceptable deviations. However, further improvements are needed to make better predictions, especially for saturated hydraulic conductivity. Particularly, micropores <10 μm were not detected due to the limitations of the MFXCT system used in this study. These micropores should be analyzed and linked to the estimation of mass transport parameters.

4. CONCLUSIONS

The pore network structures of AAC from Japan and Vietnam (typical macropore diameter >10 μm) were visualized and analyzed by using an MFXCT system. Furthermore, the correlations between mass transport parameters of AAC such as gas diffusivity, air permeability, and saturated hydraulic conductivity were examined by comparing the measured and estimated mass transport parameters from MFXCT analysis. The results of MFXCT analysis revealed that the AAC blocks from Vietnam had less tortuous macropores with smaller and narrower radii than Japanese AAC. The estimated D_p/D_0 values fitted the measured values well for all tested samples, but the estimated k_a and K_s from MFXCT under- or overestimated the measured values. The MFXCT system is able to visualize non-destructively the three-dimensional characteristics of pore geometry of porous materials and to assess pore structural parameters quantitatively. Therefore, application of the system is encouraged for characterizing construction materials.

5. ACKNOWLEDGEMENTS

This research was supported by JST-JICA Science and Technology Research Partnership for Sustainable Development (SATREPS) project (No. JPMJSA1701).

6. REFERENCES

[1] Boggelen V.W. and Boggelen V.J. Sustainable building solutions with new generation autoclaved aerated concrete panel applications. CE/papers, Vol. 2, Issue 4, 2018, pp.513-525.

[2] Matsui K., Kikuma J., Tsunashima M., Ishikawa T., Matsuno S.Y., Ogawa A. and Sato M. In situ time-resolved X-ray diffraction of tobermorite formation in autoclaved aerated concrete: Influence of silica source reactivity and Al addition. Cem. Concr. Res., Vol. 41, Issue 5, 2011, pp. 510-519.

[3] Liu Y., Leong B. S., Hu Z.T. and Yang E.-H. Autoclaved aerated concrete incorporating waste aluminum dust as foaming agent. Const. Build. Mat., Vol. 148, 2017, pp. 140-147.

[4] Nguyen T. L., Asamoto S. and Matsui K., Sorption isotherm and length change behavior of autoclaved aerated concrete. Cem. Concr. Comp., Vol. 94, 2018, pp. 136-144.

[5] Hamamoto S., Moldrup P., Kawamoto K., Sakaki T., Nishimura T. and Komatsu T., Pore network structure linked by X-ray CT to particle characteristics and transport parameters. Soils and Foundations, Vol. 56, Issue 4, 2016, pp.676-690.

[6] Baniya A., Kawamoto K., Hamamoto S., Sakaki T., Saito T., Müller K., Moldrup P. and Komatsu T., Linking pore network structure derived by microfocus X-ray CT to mass transport parameters in differently compacted loamy soils. Soil Research,Vol. 57, Issue 6, 2019, pp.642-656.

[7] Baniya A., Matsuno A. and Kawamoto K. Characterizing pore-structural parameters of volcanic ash soil: comparison between non-destructive and indirect methods. International Journal of GEOMATE, Vol. 18, Issue 69, 2020, pp.59-66.

[8] Brutsaert W. Probability laws for pore-size distributions. Soil Science,Vol. 101, Issue 2, 1966, pp.85-92.

[9] Sakaki T. and Illangasekare T. H. Comparison of height-averaged and point-measured capillary pressure–saturation relations for sands using a modified Tempe cell. Water Resources Research,Vol. 43, Issue 12, 2007.

[10] Luo L., Lin H. and Li S. Quantification of 3-D soil macropore networks in different soil types and land uses using computed tomography. Journal of Hydrology, Vol. 393, Issue 1-2, 2010, pp. 53-64.

[11] Paradelo M., Katuwal S., Moldrup P., Norgaard T., Herath L., and de Jonge L.W., X-ray CT-Derived Soil Characteristics Explain Varying Air, Water, and Solute Transport Properties across a Loamy Field. Vadose Zone Journal,Vol. 15, Issue 4, 2016.

[12] Buckingham E., Contributions to Our Knowledge of the Aeration of Soils, U.S. Government Printing Office,1904.

[13] Kozeny, J. Uber Kapillare Leitung der Wasser in Boden. Royal Academy of Science, Vienna, Proc. Class I, Vol. 136, 1927, pp. 271-306.

[14] Carman, P. C. Fluid flow through granular beds. Transactions of the Institution of Chemical Engineers, Vol. 15, 1937, pp. 150-166.